ELSEVIER

Check for
updates

Spatial and temporal variation of anthropogenic heat emissions in Colombo, Sri Lanka

Lewis Blunn [a,*], Xiaoxiong Xie [b], Sue Grimmond [a], Zhiwen Luo [b,g], Ting Sun [a,c], Narein Perera [d], Rangajeewa Ratnayake [e], Rohinton Emmanuel [f]

[a] Department of Meteorology, University of Reading, Reading, UK
[b] School of the Built Environment, University of Reading, Reading, UK
[c] Institute for Risk and Disaster Reduction, University College London, London, UK
[d] Department of Architecture, University of Moratuwa, Sri Lanka
[e] Department of Town and Country Planning, University of Moratuwa, Sri Lanka
[f] The Research Centre for Built Environment Asset Management, Glasgow Caledonian University, Glasgow, UK
[g] Welsh School of Architecture, Cardiff University, Cardiff, UK

ARTICLE INFO

ABSTRACT

Anthropogenic heat emissions (AHEs) should be accounted for when making city, neighbourhood, and building scale decisions about building design, health preparedness (e.g. heat stress), and achieving net zero carbon. Therefore, datasets with spatial and temporal variations are required for the range of global cities, including lower-middle income, low-latitude cities. Here we estimate the 2020 AHEs at 100 m resolution for Colombo, Sri Lanka. The city-wide annual mean is 5.9 W m^{-2}. Seasonal variations are very small linked to small temperature differences, unlike mid- and high-latitude cities. However, the diurnal range of 17.6 to 1.8 W m^{-2} has three distinct peaks (cf. two often found in mid-latitude cities). Transport, metabolic and building related emissions account for 35, 33, and 32% of the total emissions, respectively. Building emissions are proportionally small (cf. mid-latitudes), as there is neither need for space heating nor frequent use of air conditioning, and little heavy industry. The AHE spatial heterogeneity is large, with annual-average maxima of 124 W m^{-2} at hectometre scale, but dropping rapidly to 10 W m^{-2} at kilometre scale. City-wide projections of AHEs from 2020 to 2035 range between 24 and 61% increase.

1. Introduction

Anthropogenic heat emissions (AHEs) can play a crucial role in shaping the urban climate when solar radiation receipt is low (e.g. winter time) at high latitudes resulting in space heating needs (Hinkel et al., 2003; Hamilton et al., 2009). In summer, already warm temperatures can be exacerbated by air conditioning (AC) usage, with near-surface air temperature increases of the order of ~1 °C (e.g. Ichinose et al., 1999; Bohnenstengel et al., 2014; Xie et al., 2016; Takane et al., 2020; Xue et al., 2020). In the low-latitudes AHEs tend to be less than at higher latitudes (Flanner, 2009; Allen et al., 2011), because of reduced wintertime space heating needs associated with warmer air temperatures (Grimmond, 1992; Sailor and Lu, 2004; Pigeon et al., 2007). Warm season use of AC tends to vary with

---

financial resources, with lower-income countries less likely to prioritize AC (Allen et al., 2011). Whereas in high-income counties AC usage can be large (e.g. Singapore (Quah and Roth, 2012)). Hence, in low-latitude cities the anthropogenic heat flux from buildings ($Q_{F,B}$) is often a smaller fraction of total anthropogenic heat flux (Q_F) (cf. higher latitude cities).

Q_F varies not only with latitude but between countries. Stewart and Kennedy (2017) found that metabolism ($Q_{F,M}$) accounted for only 4–8% of Q_F in mid-latitude cities (e.g. London, Tokyo, New York), but in low-latitude cities (e.g. Cairo, Dhaka, Kolkata) it can be 10–45%. This is consistent with Allen et al. (2011) estimates of 30–72% in low-latitude African cities, which are attributed to high population densities (Dong et al., 2017), but also low emissions from vehicles ($Q_{F,V}$) and buildings ($Q_{F,B}$). Stewart and Kennedy (2017) estimate $Q_{F,V}$ in high-income North American, East Asian, and Western European cities where private ownership of vehicles is common to be 25–31% of Q_F, but drops to 15–17% in South Asia and Africa.

Variation also occurs across cities, with larger values in the central business district (CBD) cf. outer areas (e.g. Chengdu, Chongqing (Ming et al., 2021)). The urban form, building usage, population density, and transport network all vary at both kilometre and sub-kilometre scales (Gabey et al., 2019). There are also large temporal variations in emissions because of changes in activities (e.g. diurnal, day of week). AHEs need to be considered for a variety of city activities across many spatial scales (city wide, neighbourhood, building) when decisions are made about long term planning (e.g. local building design, neighbourhood planning), both for future climate and day-to-day operations (e.g. overheating impacting health preparedness and energy infrastructure). Increasingly O(100 m) grid length numerical weather prediction (NWP) is being used to understand urban climates at neighbourhood scales (Ronda et al., 2017; Leroyer et al., 2022). Q_F makes a significant contribution to the surface forcing in such models (Bohnenstengel et al., 2014). However, current Q_F inventories covering lower-latitude, low to lower-middle income countries tend to be kilometre-scale, lacking sub-km information on Q_F dynamics, and are largely based on country level energy consumption data.

In hot low-latitude cities, people may be exposed to high, and increasingly extreme heat stress, both outdoors (Coffel et al., 2017) and indoors (Adunola, 2014; Ramsay et al., 2021). Low and lower-middle income cities are likely to undergo large changes in building stock and human activity in the coming years as there is increasing urbanisation (UN, 2019). With increasing household income more energy may be consumed in buildings and for transport. How cities house increasing urban populations may vary between construction of tall buildings and sprawl, creating larger transport needs. The directions taken will depend on policy (at various levels) and economic growth amongst many other uncertainties. As cities compare options to make them more resilient and prepare (e.g. net zero-carbon options) it is essential to have benchmark Q_F data to assess possible feedbacks between options being considered.

The objective of this paper is to determine the spatial and temporal variability of a major lower-middle income city in the tropics. The influence of local climate zone (Stewart and Oke, 2012), neighbourhood type, and grid length are considered. We focus on Colombo, Sri Lanka (Fig. 1), which already experiences extreme temperatures and is expecting urban growth with projections for 2035 (land cover, population, and transport) already existing as scenarios. We calculate (Section 3.4) and analyse magnitude, diurnal variation, and spatial variation of the Q_F components (Section 4.1–4.3) for 2020, investigate the influence of grid length (Section 4.4), and make projections for the future (2035) (Section 4.5).

2. Parametrization of anthropogenic heat flux

The three major sources of anthropogenic heat flux (Q_F) are heat emissions from metabolism ($Q_{F,M}$), buildings ($Q_{F,B}$), and transport ($Q_{F,V}$) (Grimmond, 1992):
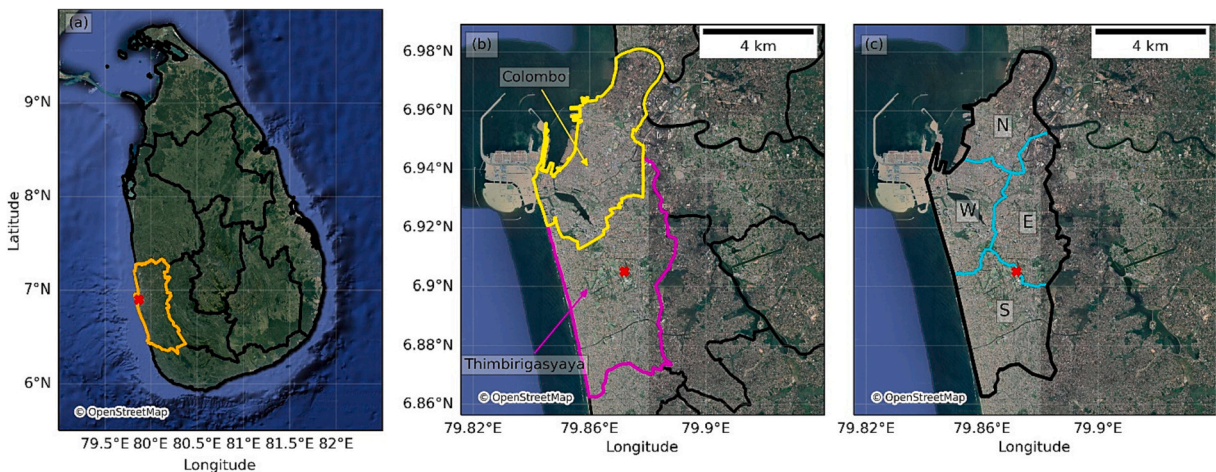
Fig. 1. Key regions in this study: (a) Western province (orange) and other provinces in Sri Lanka (black) (b) divisional secretariat boundaries (black) including Colombo (yellow) and Thimbirigasyaya (magenta), (c) N, S, E, and W (cyan) electricity consumption regions (Table 2) within the CMC (black lines) and location of the Colombo Meteorological Observatory (6.905°N, 79.872°E, red). Base imagery: OpenStreetMap contributors (2021). (For interpretation of the references to colour in this figure legend, the reader is referred to the web version of this article.)

$$Q_F = Q_{F,M} + Q_{F,B} + Q_{F,V} \tag{1}$$

Heat released by metabolism of animals and people vary with activity (e.g. cycling versus sitting or sleeping). In buildings, the energy uses include cooking, appliances and lighting. Many modes of transport (e.g. cars, buses, trucks) release energy from combustion.

A common simple, dynamic approach used for determining Q_F in mid- and high-latitude cities is as a function of air temperature relative to local heat and cooling thresholds captured by heating (HDD) and cooling degree days (CDD) (Sailor and Vasireddy, 2006):

$$Q_F = \rho(a_0 + a_1 CDD + a_2 HDD) \tag{2}$$

This allows for variations in population density (ρ) and local socio-economic-cultural conditions (a_0, a_1, and a_2) which may vary by day type (e.g. Järvi et al., 2011) and across a mega-city (e.g. Ward and Grimmond, 2017). The a_0 parameter accounts for the temperature independent energy use from all three sources of Q_F.

In Eq. 2, a_1 parameterises the summertime energy use response, notably increased building cooling with warmer conditions. Similarly, a_2 accounts for wintertime response, most notably linked with increased building heating with colder temperatures. All three parameters can be explicitly expanded to be more responsive (Allen et al., 2011; Lindberg et al., 2013; Stewart and Kennedy, 2017), as especially in low-latitude cities, $Q_{F,M}$, $Q_{F,V}$, and $Q_{F,B}$ all make large contributions to Q_F (Stewart and Kennedy, 2017).

If there are no large variations in temperatures modifying energy consumption through the year, the last two terms of Eq. 2 are not needed (i.e. $a_1 = a_2 = 0$). Hence, for low latitudes, after expanding the remaining a_0 and ρ terms in Eq. 2 to account for the three components in Eq. 1 we have:

$$Q_F(t_h i) = \left[\rho\left(t_{h,\{wdwe\}}\right) a_{0,M}(t_h) \right] + \left[\rho\left(t_{h,\{wdwe\}}\right) \left\langle a_{0,B}\left(t_{h,\{wdwe\}}\right) \right\rangle_r \right] + \left\langle a_{0,V}\left(t_{h,\{wdwe\}}\right) \right\rangle_r \tag{3}$$

where the subscripts M, B, V, wd and we correspond to metabolic, building, transport, workdays, and non-workdays, respectively. Given spatial units, or regions (r), differ between the datasets used to constrain the three components being downscaled, their number and locations vary (e.g. Fig. 1). The total flux $Q_F(t_h, i)$ is calculated for each timestep (t_h, i.e. hourly, h) for each individual grid (i). The grid subscript is dropped from the notation on the right-hand side for clarity.

The metabolism varies diurnally ($t_{h,\{wd,we\}}$) by type of day as large behavioural changes occur between work (wd) and non-workdays (we) (e.g. Kotthaus and Grimmond, 2012; Capel-Timms et al., 2020). On workdays people need to commute to and from work, before and after their work period, whereas at night people tend to be asleep. Thus, the metabolism varies with probable behaviour or activities and number of people within an area (grid cell i) at a time ($t_{h,\{wd,we\}}$).

Metabolism rate ($a_{0,M}(t_h)$) can be related to food consumption based on local 24-h recall survey estimates (e.g. Jayatissa and Marasingha, 2022). Diurnal variations can be estimated using generic metabolism ratios between awake and asleep (ratio = 2.3, Sailor and Lu, 2004) with values linearly changing as the fraction of people asleep varies. We assume animal metabolism is negligible as they contribute <1% of emissions in the 26 cities Stewart and Kennedy (2017) studied.

The population density varies with day type and time of day because of people's activities. Residential locations, where people are at night on workdays or on non-workdays, are the data provided (and constrained) by census data. Ideally the highest spatial resolution of the official data is used. To determine workday population densities census data may also be available. The timing of travel can inform the likely sub-daily pattern (Section 3.3).

For building energy consumption, monthly regional building flux ($\left\langle a_{0,B}(t_m) \right\rangle_r$) are used to calculate the annual mean ($\left\langle a_{0,B}(t_a) \right\rangle_r$), which are downscaled to hourly values $\left\langle a_{0,B}\left(t_{h,\{wd,we\}}\right) \right\rangle_r$ using a diurnal profile (diurnal mean of 1) for electricity consumption in Sri Lanka $\widehat{b}_d(t_h)$ and the population density on wd and we:

$$\left[\rho\left(t_{h,\{wdwe\}}\right) \left\langle a_{0,B}\left(t_{h,\{wdwe\}}\right) \right\rangle_r \right] = \left\langle a_{0,B}(t_a) \right\rangle_r \left[\frac{\widehat{b}_d(t_h)\rho\left(t_{h,\{wdwe\}}\right)}{\overline{\widehat{b}_d(t_h)\rho\left(t_{h,\{wdwe\}}\right)}} \right] \tag{4}$$

where the overbar in the denominator represents the annual average. We assume it is reasonable to approximate energy consumption as instantaneously being converted to outside heat emissions in Colombo, as building ventilation rates are high compared to Europe (8 air changes per hour (Xie et al., 2024a) cf. 1 air changes per hour (Dimitroulopoulou, 2012)). For cities with significant industry (unlike Colombo, Section 3.4), using non-domestic land use with building energy consumption data would improve spatial downscaling. Where there is widespread space heating and air conditioning (AC) (unlike Colombo, Section 3.4), such as in many mid- and high-latitude cities (e.g. Sailor and Vasireddy, 2006; Järvi et al., 2011, Ao et al., 2018), it would be beneficial to have the daily air temperature – building heating/cooling related energy consumption response functions (e.g. Eq.2) included.

The average daily heat emission from vehicles for a day is a function of the area of region (A_r, m^2), mode of transport (j, e.g. car, bus), fuel consumption (F_{C-g}^j, L km^{-1}) and distance travelled (D, km):

$$\left\langle a_{0,V}\left(t_{d,\{wd,we\}}\right) \right\rangle_r = \frac{E_G}{A_r N_{s/d}} \sum D_{\{wd,we\}}^j F_{C-g}^j \tag{5}$$

where $N_{s/d}$ and E_G are the number of seconds in a day and the energy released by combustion of gasoline (32 MJ L^{-1}; (EC, 2017)). The regional journey data are downscaled to the individual grids assuming that the emissions are proportional to the area of road in the grid ($A_{road,i}$), with all areas having the same characteristics, and are downscaled to hourly values based on diurnal profiles of trips

$\widehat{v}\left(t_{h,\{wd,we\}}\right)$ (diurnal mean of 1):

$$\left\langle a_{0,V}\left(t_{h,\{wd,we\}}\right)\right\rangle_i = \frac{A_{road,i}}{A_{road,r}}\left\langle a_{0,V}\left(t_{d,\{wd,we\}}\right)\right\rangle_r \widehat{v}\left(t_{h,\{wd,we\}}\right) \tag{6}$$

The downscaling of train emissions follows the same equation except the road area is replaced by track length.

3. Methods

3.1. Study area

The Sri Lankan commercial capital, Colombo city (37 km^2) (black line, Fig. 1c, 6.92°N, 79.85°E) has a large area of suburbs, 110 km^2 of which is included in the study (region outside of black line, Fig. 1c). In Sri Lanka, the administrative structure consists of provinces subdivided into districts with sub-units referred to as divisional secretariats, that are divided into grama niladhari (village officer) divisions. The Western Province (orange line, Fig. 1a) has 13 divisional secretariats (one called Colombo, which has 35 grama niladhari sub-units). The Colombo city region has both the Colombo and Thimbirigasyaya divisional secretariats (Fig. 1b). The Colombo divisional secretariat is distinct from the Colombo city region defined by the Colombo Municipal Council (CMC, Fig. 1c). Herein we use Colombo to refer Colombo city unless in the context of divisional secretariats.

The regional climate is classified as Koppen-Geiger tropical rainforest (Beck et al., 2018). There is little seasonal variation in temperature and humidity, and rainfall occurs year-round (Emmanuel and Johansson, 2006; Perera and Emmanuel, 2018). Monthly mean daily maximum and minimum near surface air temperatures are 30–32 °C and 22–26 °C, respectively (Emmanuel and Johansson, 2006).

3.2. Land cover characteristics

Land cover data are needed not only to calculate Q_F, but also to undertake broader climate modelling to provide the datasets required for building design (Xie et al., 2024b). The spatial analysis (Fig. 2) is undertaken using a 100 m grid to obtain six land cover types (building, paved, trees, grasses, bare soil and water) fractions and morphology (Table 1). As next generation numerical weather prediction will likely be run at hectometric grid lengths, it is important to understand Q_F at this scale. For understanding building
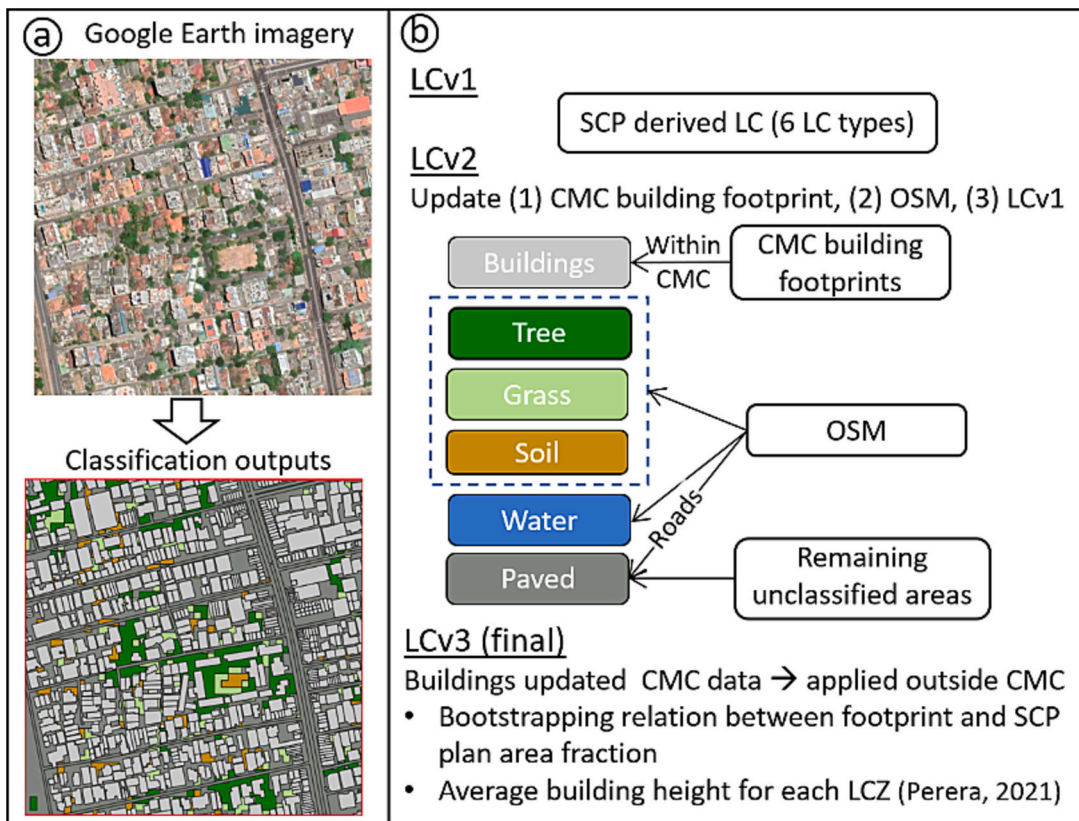

Fig. 2. Land cover fraction calculation (b) procedures and (a) example outputs.

settings, we want to have detailed information while ensuring there are multiple buildings per grid cell. It will, for example, be rare to have a single large building occupying the entire grid cell, leading to a building fraction of 1, which is unsuitable for use in surface energy balance models. See Section 4.4 for further discussion on the influence of grid length on Q_F.

An iterative process is employed which first uses the Semi-Automatic Classification Plugin (SCP) (Congedo, 2021) in QGIS (QGIS Development Team, 2022) and a clear sky Sentinel-2 multiband (20 m resolution) satellite image (ESA, 2018) taken on 20 February 2020 covering the study area (Fig. 1b). The SCP algorithm training involved visual inspection of high-resolution satellite imagery (Google, 2022) at 60 samples across the Sentinel-2 image, allowing SCP to generate the first version of a land cover map (LCv1).

To improve LCv1 additional data are used:

- *Buildings* – CMC building footprints and number of storeys (Blunn et al., 2022) are used to derive the volumes with heights obtained by assuming the 3 m minimum storey height regulation (UDA, 2018) plus 1 m to account for roof height.
- *Roads (paved)* – To determine the area of roads (A_{road}) the OpenStreetMap (OpenStreetMap contributors, 2021) roads are used. By inspection of Google Earth imagery (Google, 2022) at 10 random locations per road class (24 classes) the road width of each class is estimated. To avoid areal overestimation, the class minimum width is used with the OpenStreetMap line features.
- *Trees and grass* – OpenStreetMap's 16 vegetation types in Colombo do not include scattered vegetation (e.g. street trees). After inspecting imagery (Google, 2022) the 16 classes are assigned to our two classes (Table SM.1). The SCP identified scattered vegetation is retained.
- *Bare soil* – OpenStreetMap railways are classified as bare soil.
- *Water* – OpenStreetMap has 'large open water' (e.g. lakes, rivers, and pools) polygons, and narrow waterways (e.g. canals and streams) as lines. To obtain areas for the latter, the same approach as roads is used.

These data are used to update the LCv1 based on the following order of assumed accuracy: (1st) buildings, (2nd) land cover derived from OpenStreetMap, and (3rd) SCP LCv1 results. Paved fraction is equal to the sum of road fraction and the remaining unclassified areas, based on visual inspection of ESA. This version is LCv2.

To improve the estimate of building fraction beyond the CMC area, within the CMC area bootstrapping is applied to obtain a plan area fraction relation between CMC building footprints and SCP data (Section SM2). This relation is applied to correct the SCP data outside the CMC. To extend the building height information beyond the CMC, within the CMC mean building heights are calculated (Fig. SM.2) for local climate zones (LCZs), as mapped by Perera (2021) (Fig. 3d). This results in any uncertainties from the LCZ mapping being retained. For example, LCZ1 (Compact – high-rise, Table 4) building heights are the mean of CMC footprint building height for all LCZ1 grid cells (17.0 m), which suggests some areas are misclassified.

The calculated values are assigned beyond the CMC using the LCZ map. Other building height relations assessed had weak relations so are not used (Fig. SM.3).

3.3. Population characteristics

Population densities are used to weight the different anthropogenic heat flux terms (Section 2). This allows for difference by day type (workday, *wd;* non-workday, *we*) and time of day. A typical working week is Monday-Friday (Sri Lanka Travel Guide, 2022). All times referred to are local standard time (LST), UTC +5.5.

In 2012 based on divisional secretariats census data, the Colombo population (i.e. within the CMC) was 0.578 million. The United Nations (UN) estimate of Colombo population for 2020 is 0.613 million (UN, 2019). To adjust for this growth the 2012 population densities in each divisional secretariat are scaled by 1.061(=0.613/0.578) so that the population density in 2020 equals the UN estimate. The 2020 nocturnal (residential) population density (ρ_{noc}) was 146 capita ha^{-1} in Colombo and during the daytime on workdays 269 capita ha^{-1} (Dept. of Census and Statistics, 2012), with the larger daytime density linked to people commuting into Colombo for work. The typical workday period, based on timing of trips to and from work in the Western Province (JICA (2014), their Fig. 3.1.23), is assumed to linearly increase from 04:00–10:00 LST and vice-versa in the evening between 16:00–22:00 LST (Fig. 4a).

Table 1
Land cover and population datasets used.

| Type	Dataset	Region	Reference
Building	Number of storeys (2014)	CMC	Building GIS data (Urban Development Authority, Sri Lanka prepared by Survey Dept. of Sri Lanka) (Blunn et al., 2022)
	CMC building footprint (2014)	CMC	Building GIS data (Urban Development Authority, Sri Lanka prepared by Survey Dept. of Sri Lanka) (Blunn et al., 2022)
Population	Density (2012)	Divisional secretariats	Social Administrative GIS data (Blunn et al., 2022) based on the Census of Population and Housing, 2012, Sri Lanka (Dept. of Census and Statistics, 2012).
Road	Area	–	OpenStreetMap contributors (2021)
	Width	–	Google (2022)
Water	Area	–	OpenStreetMap contributors (2021)
	Width (narrow waterways)	–	Google (2022)
Bare soil	Area	–	Sentinel-2 multi-band satellite data (ESA, 2018)
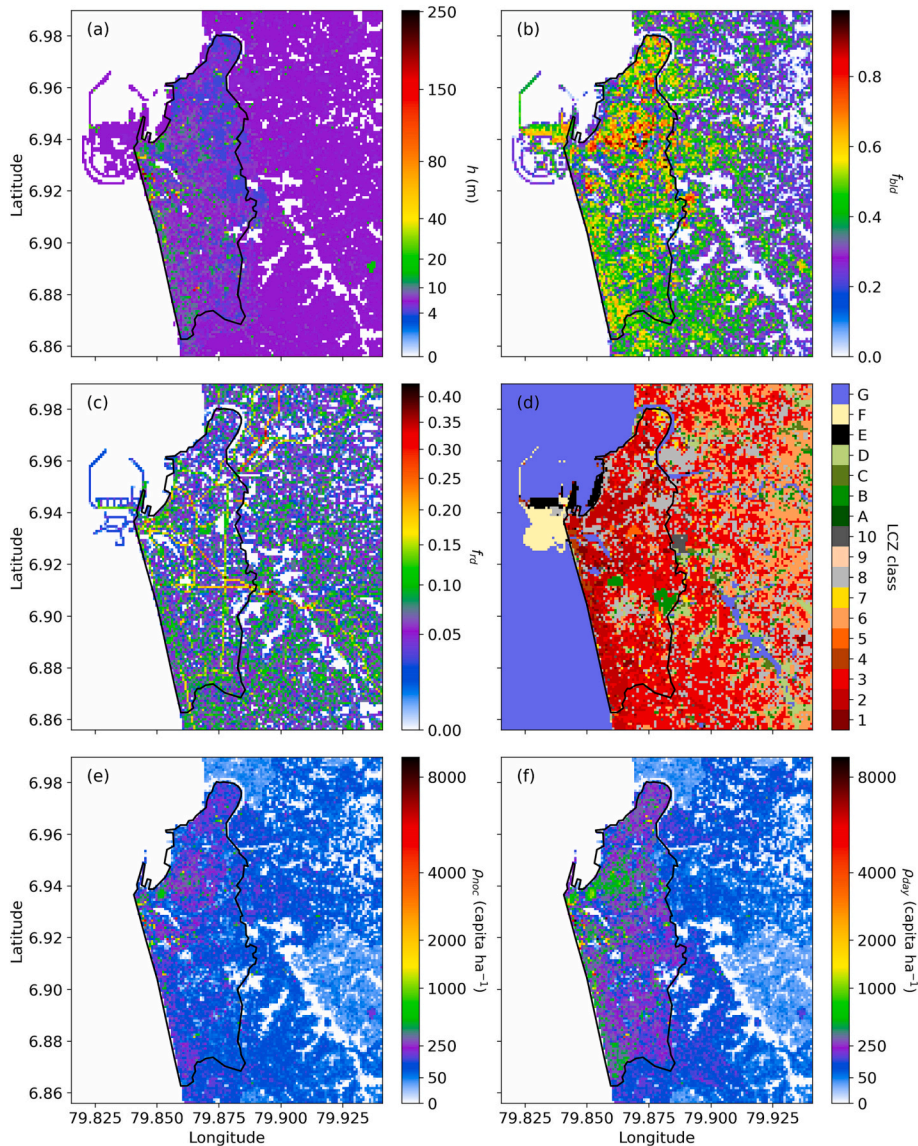
Fig. 3. Colombo Municipal Council (CMC, black line) and surrounding study area mapped at 100 m grid resolution (Section 3), showing: (a) mean building height (h), (b) plan area fraction of buildings (f_{bld}), (c) plan area fraction of road (f_{rd}) (i.e. part of the paved land cover fraction), (d) Perera (2021) local climate zones (LCZs, Table 4) derived using the Demuzere et al. (2021) application, and population densities for (e) nocturnal and non-workday daytime (ρ_{noc}) and (f) daytime workday (ρ_{day}). All colour bars except (d) have logarithmic scale.

We assume no commuting occurs on non-workdays so the population density remains equal to ρ_{noc} to give the different *wd* and *we* profiles (Fig. 4a).

Spatial variability in population density at 100 m grid scale is based on conserving the divisional secretariat totals (Dept. of Census and Statistics, 2012) assuming it is proportional to building volume. Hence, the resulting densities (Fig. 3e,f) are largest in the 100 m (or 1 ha) grid cells with tall buildings (Fig. 3a) and large building fractions (Fig. 3b). The maximum night-time or *we* density is 5437 capita ha^{-1} for a grid cell with a mean building height (h) of 194 m and building fraction (f_{bld}) of 0.48. The Colombo divisional secretariat average ρ_{noc}, h, and f_{bld} are 192 capita ha^{-1}, 8.0 m, and 0.42, respectively. Hence, the extreme ρ_{noc} grid cell building volume is 28 times larger than the Colombo divisional secretariat average volume.

3.4. Anthropogenic heat flux (Q_F)

To calculate the time and space varying Q_F (Eq. 3) for the Colombo area we use local data to constrain the three Q_F components.

For metabolism, we use Jayatissa and Marasingha (2022) food consumption value (2068 kcal capita^{-1} day^{-1}) estimated using the 24-h recall method. This per person mean in a household is derived from a representative sample of Sri Lankans aged 6 months to 95
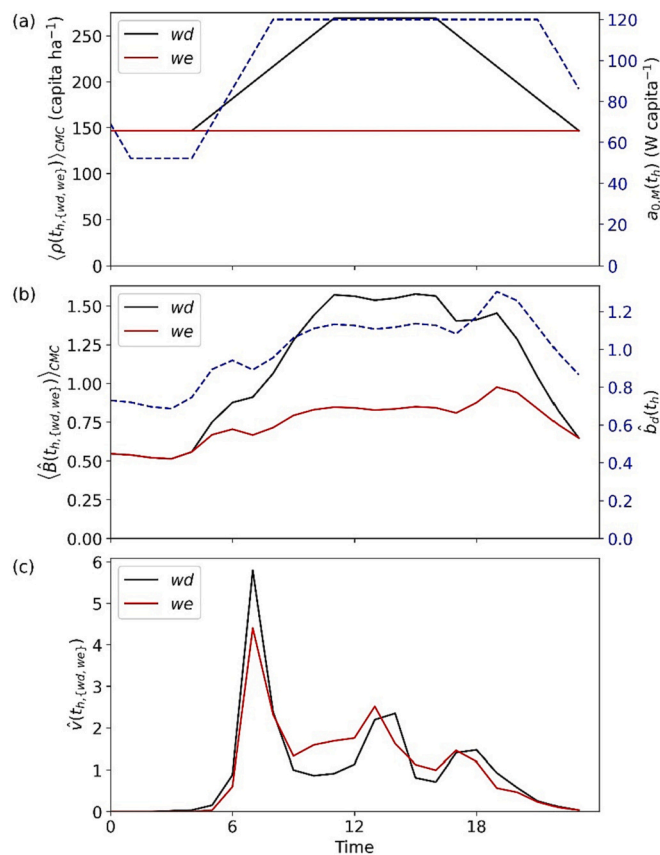
Fig. 4. Diurnal variation in Colombo, by day type (workdays, *wd*; non-workdays, *we*) of: (a) population density (left Y-axis), and metabolic power output per person (right Y-axis, dashed), (b) building emissions normalised by annual-mean for Colombo (term in square brackets on right hand side of Eq. 4) (left Y-axis) and diurnal profile of electricity consumption normalised by daily average for Sri Lanka (right Y-axis, dashed), and (c) combustion from motorised vehicles scaled by daily-mean. Source: JICA (2014, their Fig. 3.1.23). For the model formulation and data methods and sources see Sections 2 and 3, respectively.

years. Estimates of uncertainty in Sri Lankan food consumption are informed by Jayawardena et al. (2014) similar study which estimates food consumption of adults (>18 years) to be 1714 kcal capita^{-1} day^{-1} and the FAO (2012) South-Asian projection of food consumption estimates of 2420 and 2590 kcal capita^{-1} day^{-1} for 2015 and 2030, respectively. We consider Jayatissa and Marasingha (2022) estimate most plausible, as 1714 kcal capita^{-1} day^{-1} is below the minimum food rations required (1900 kcal capita^{-1} day^{-1}) for displaced people (Mason, 2002), whilst the FAO (2012) regional top-down estimate uses (non-Sri Lankan) production, imports and exports.

Assuming a 2.3 awake to asleep metabolism ratio (Section 2) gives a daytime $a_{0,M}$ of 120 W capita^{-1} and a sleeping value of 52 W capita^{-1} (blue dashed, Fig. 4a). To split the remainder of the day, the timing of trips (e.g. to school, work, home after work) (JICA (2014), their Fig. 3.1.23) is determined by the assumption that people sleep for 7 h. The fraction of people asleep is set to increase linearly from 1 to 0 between 04:00–08:00 and increasing fraction asleep from 0 to 1 between 21:00–01:00. The workday and non-

Table 2
Monthly values for December 2017 to March 2018 of: (a) electricity consumption (Source: Ceylon Energy Board (CEB), obtained by request) by region and (b) near surface temperature (Source: NOAA, 2001). Fig. 1c shows locations.

	Region/Location	Electricity consumption (MWh)			
		Dec 2017	Jan 2018	Feb 2018	Mar 2018
(a)	CEB North (N)	7636	7719	7482	7993
	CEB South (S)	10,680	10,843	10,890	11,331
	CEB East (E)	9794	10,154	9809	10,579
	CEB West (W)	7781	7906	7808	8208
	Total	35,891	36,622	35,989	38,111
(b)	Colombo Meteorological Observatory				
	(6.905°N, 79.872°E) Air temperature (°C)	27.0	26.6	31.9	28.2

workday differences are driven by population density differences (Section 3.3).

The monthly electricity data (Table 2) varies between 35.9 and 38.1 GWh in the four-month period (Table 2) while the mean near-surface air temperature varies between 26.6 and 31.9 °C (Table 2). There is no correlation between electricity consumption and temperature (Table 2). This suggests that with air temperatures rarely below 20 °C (Emmanuel and Johansson, 2006) that energy is seldom used for space heating, and that variations in AC usage make little (or small) contribution to electricity consumption. This is consistent with Stewart and Kennedy (2017) estimate for other low to lower-middle income (WB, 2022), low-latitude cities (Kolkata, Delhi, Karachi, and Dhaka) with very low electricity consumption (1.2–2.7 W m^{-2}) attributed to negligible space heating and use of natural ventilation rather than AC given the high cost of electricity. Hence, the two last terms of Eq. 2 are omitted, and Eq. 3 is used. Also, given there is little variation in electricity consumption between the four months, the data is used to estimate annual electricity consumption in the four Ceylon Energy Board (CEB) regions for 2020.

Sri Lanka household income and expenditure surveys (in 2012/2013) find energy consumption is split between electricity (63%), kerosene (14%), liquified petroleum gas (14%), and firewood (8%) (Pallegedara et al., 2021). Natural gas is not a component of the energy mix in Sri Lanka (SLSEA, 2017). Although electricity produced by photovoltaics installed on individual buildings can be sold back to the grid (Jayaweera et al., 2018), it is not included in the CEB electricity consumption data (Table 2). However, as photovoltaics account for ~0.01% of Sri Lanka's electricity demand (Jayaweera et al., 2018), we make no adjustments. Therefore, assuming energy efficiency is the same and Pallegedara et al. (2021) results hold for all buildings in Colombo, the electricity consumption is scaled by 1.59(=100/63). Building emissions, therefore, refer to the sum of electricity (63%) and other (kerosene, gas, firewood, etc.) (37%). As industrial electricity consumption is <1.2% of the CEB total electricity consumption in Colombo (Ceylon Energy Board (CEB), obtained by request, Blunn et al., 2022), the spatial variation of building emissions are not strongly controlled by industry.

The diurnal variation of building emissions is estimated using Sri Lanka's electricity load profile for the day where peak electricity consumption occurred in 2017 (SLSEA (2017), their Fig. 6.3) but the profiles do not vary much with the year (SLSEA (2017), their Fig. 6.3). Peak electricity load (and therefore peak Sri Lanka building emissions) tends to occur at 19:00 when people return home, cook and undertake some recreation activities (blue dashed, Fig. 4b). The population density is used to weight the building emissions. The peak building emissions in Colombo on workdays is at 15:00 (black solid, Fig. 4b), when large building emissions (blue dashed, Fig. 4b) coincide with peak population density in Colombo (black solid, Fig. 4a).

For transport emissions, the regional constraints are journey data for the Western Province (orange, Fig. 1a) which are summarised in Table 3. The total area of Colombo Municipal Council or Colombo City (CMC, black, Fig. 1c) is $A_{r=CMC} = 37$ km^2. On *wd* the diurnal variation of vehicle emissions is assumed proportional to the *wd* diurnal variation of total number of trips in the Western Province of Sri Lanka (JICA (2014), their Fig. 3.1.23) (black, Fig. 4c). On *we* the diurnal variation (red, Fig. 4c) is found by subtracting the work and school related trips (JICA (2014), their Fig. 3.1.23) from the *wd* trips.

4. Results and discussion

4.1. Magnitude and temporal variation of anthropogenic heat flux (Q_F)

The 100 m resolution annual mean Q_F in Colombo for 2020 is 5.9 W m^{-2} (Table 4). This is consistent with equivalent values in other low- and lower-middle income, low-latitude cities in Asia (Stewart and Kennedy, 2017) and Africa (Allen et al., 2011); and in Colombo for 2010 at 1 km resolution (6.1 W m^{-2}, Varquez et al., 2021) (Table 4).

At 100 m, the annual mean component sources in decreasing size are from transport (2.0 W m^{-2}), metabolism (2.0 W m^{-2}) and buildings (1.9 W m^{-2}). This ordering is generally consistent with metabolism and buildings found in other low to lower-middle income, low-latitude cities (Allen et al., 2011; Stewart and Kennedy, 2017). However, Colombo is unusual in having a larger mean from

Table 3

To calculate transport related heat emission, the constraining regional data for Colombo is the Western Province (Fig. 1). The total number of trips per day (N_T) for workdays (*wd*) are estimated from JICA (2014, their Fig. 5.2.1^), with non-workdays (*we*) derived from JICA (2014, their Fig. 3.1.23§) trip purpose data after removing work and school trips. The JICA (2014, their Fig. 3.1.6) frequency of trips by modes is used to split these N_T totals by mode. An average trip length for all motorised mode of transport is assumed to be 5 km based on the E to W (~4 km) and N to S (~10 km) dimensions of Colombo. The number of people in each vehicle (N_P) are based on: † Lanka Ashok Leyland Viking (MTCA, 2018) capacity (54) but at peak times >120% capacity (JICA (2014), their Table 3.3.1) so full on average assumed; ‡ common train (Sri Lanka Class S11) seating capacity (Sri Lanka Railways (2019), their Section 7) based on most Sri Lankan train lines being Diesel Multiples Units (JICA, 2014). Gas consumption (F_{C-g}) sources: ¶ Sri Lanka Railways (2019, their Section 8); ‡ FHWA (2016, their Table VM-1); ‡ mean of motorcycles and cars.

	N_T ($\times 10^6$)		N_P	Distance ($\times 10^3$ km)		F_{C-g} (L km^{-1})	$Q_{F,V,CMC}$ (W m^{-2})	
	wd	*we*		*wd*	*we*		*wd*	*we*
Train	0.07	0.04	620‡	0.8	0.4	2.37¶	0.01	0.01
Bus	0.91	0.47	54†	84.4	43.1	0.32‡	0.27	0.14
Car	0.26	0.13	2	660.0	336.7	0.10‡	0.65	0.33
Motorcycle	0.34	0.17	1	1680.0	857.1	0.05‡	0.90	0.46
3-wheeler	0.31	0.16	2	780.0	398.0	0.07*	0.54	0.28
Walk/Bike	0.50	0.26	0/1					
Total	2.40^	1.22§					2.38	1.22

Table 4

Anthropogenic heat flux (Q_F, units W m^{-2}) and electricity (E, units W m^{-2}) from this study and the literature.

(a) Total anthropogenic heat flux (W m^{-2}) for Colombo, CMC for all days, workdays (*wd*) and non-workdays (*we*). SD and IQR stand for all days standard deviation and interquartile range, respectively.

Colombo (period)	resolution	mean	SD	Median	IQR	wd	we
Varquez et al. (2021) Q_F (2010)	1 km	6.1	6.2	3.3	5.5		
This study Q_F (2020)	100 m	5.9	5.6	5.4	3.4	6.7	4.1
Metabolism $Q_{F,M}$	100 m	2.0	3.0	1.6	1.3	2.2	1.5
Transport $Q_{F,V}$	100 m	2.0	1.6	1.8	1.9	2.4	1.2
Building $Q_{F,B}$	100 m	1.9	2.4	1.6	1.3	1.2	1.4
$Q_{F,V}/Q_{F,B}$		1.07				1.13	0.85
E		1.2				1.3	0.9

(b) Colombo Electricity regions (Dec 2017 – Mar 2018) (Fig. 1)

	Q_F	$Q_{F,M}$	$Q_{F,B}$	$Q_{F,V}$	E	Building Vol. /Grid Area (m^3/m^2 = m)
N	5.4	1.9	1.9	1.6	1.2	2.66
S	5.7	1.6	1.8	2.3	1.1	3.08
E	5.2	1.5	1.6	2.1	1.0	2.68
W	7.6	3.1	2.4	2.1	1.5	4.45

(c) Colombo fluxes for 2020 by LCZ, with heights derived for each LCZ (methods given in section 3.2)

Local climate zone (LCZ)		Q_F	$Q_{F,M}$	$Q_{F,B}$	$Q_{F,V}$	$Q_{F,B}/Q_{F,M}$	Height (m)
Compact – high-rise	1	10.4	4.2	3.8	2.4	0.89	17.0
Midrise	2	7.3	2.5	2.4	2.4	0.96	7.7
Low-rise	3	5.3	1.6	1.7	2.0	1.03	6.5
Open – high-rise	4	13.2	6.1	4.9	2.2	0.81	25.7
Midrise	5	6.4	1.8	1.8	2.8	0.99	8.2
Low-rise	6	3.4	1.0	1.1	1.3	1.06	6.5
Lightweight – low-rise	7	5.1	1.7	1.7	1.7	1.01	4.9
Large – low-rise	8	4.7	1.4	1.4	1.9	0.99	6.1

(d) Annual mean fluxes Colombo for 2035. Details of projections (P) given in Table 6: relative size of increase indicated by ↑

Pop	Building vol	Trips	P	Q_F	$Q_{F,M}$	$Q_{F,B}$	$Q_{F,V}$	V/B	E
↑	-	↑	P1	7.4	2.5	2.4	2.6	1.08	1.5
↑↑	↑↑↑	↑	P2	8.9	3.3	3.0	2.6	0.86	1.9
↑↑	↑↑↑	↑-cars	P3	9.5	3.3	3.0	3.2	1.08	1.9
↑↑	↑↑↑	↑-bus/train	P4	8.5	3.3	3.0	2.2	0.74	1.9
↑	↑	↑	P5	7.5	2.5	2.5	2.6	1.03	1.6

(e) Annual mean for period indicated in other low to lower-middle income, low-latitude cities.

		Q_F	$Q_{F,M}$	$Q_{F,B}$	$Q_{F,V}$	$Q_{F,V}/Q_{F,B}$	E
Asia	Kolkata	7.7	3.5	3.0	1.1	0.37	2.7
	Delhi	8.6	2.0	3.7	2.8	0.76	2.2
Stewart and Kennedy (2017) for 2011	Karachi	6.1	1.0	4.2	0.8	0.19	1.2
	Dhaka	16.1	2.3	13.3	0.5	0.04	1.2
Africa	Ouagadougou	< 3					
Allen et al. (2011) for 2005	Lagos	< 9					
	Kinshasa	< 3					

transport ($Q_{F,V}$) than building ($Q_{F,B}$) sources (Table 4). Comparison of $Q_{F,V}/Q_{F,B}$ ratios (Table 4) indicate Colombo is most similar to Delhi. These cities (Stewart and Kennedy, 2017) have larger $Q_{F,B}$ (3.7–13.3 W m^{-2}) but generally smaller $Q_{F,V}$ (0.5–2.8 W m^{-2}) values than Colombo.

Like Karachi and Dhaka, the Colombo electricity consumption is 1.2 W m^{-2} (Table 4), but Colombo $Q_{F,B}$ (2.0 W m^{-2}) has very small space heating and industry related energy consumption, with some heat emissions from kerosene, gas, and firewood burning likely associated with cooking (Section 3.4). Whereas, $Q_{F,B}$ in both Karachi (4.2 W m^{-2}) and Dhaka (13.3 W m^{-2}) have proportionally large space heating and industry which contributes (3.1 and 12.1 W m^{-2}, respectively) (Stewart and Kennedy (2017), their Table 3).

In Colombo, the AHEs are 62% larger on workdays (*wd*) than non-workdays (*we*), linked to all components (metabolic, building, and transport) having larger AHEs (Table 4). This contrasts with high income, mid-latitude cities of London and Tokyo where AHEs are only ≈ 2% larger on *wd* than *we* (Allen et al. (2011), their Fig. 10) but this may relate to the coarse spatial scale of the latter model not capturing the details of people's transport activity. The Colombo $Q_{F,M}$ on *wd* and *we* is the same (0.8 W m^{-2}) in the middle of the night (Fig. 5). During the daytime $Q_{F,M}$ is up to 84% larger on *wd* than *we* because of commuters going to work. $Q_{F,M,\{wd\}}$ increases from 0.8 W m^{-2} at 04:00 to 3.2 W m^{-2} at 10:00 (Fig. 5a). The large diurnal variation is linked to an increase in metabolism and population
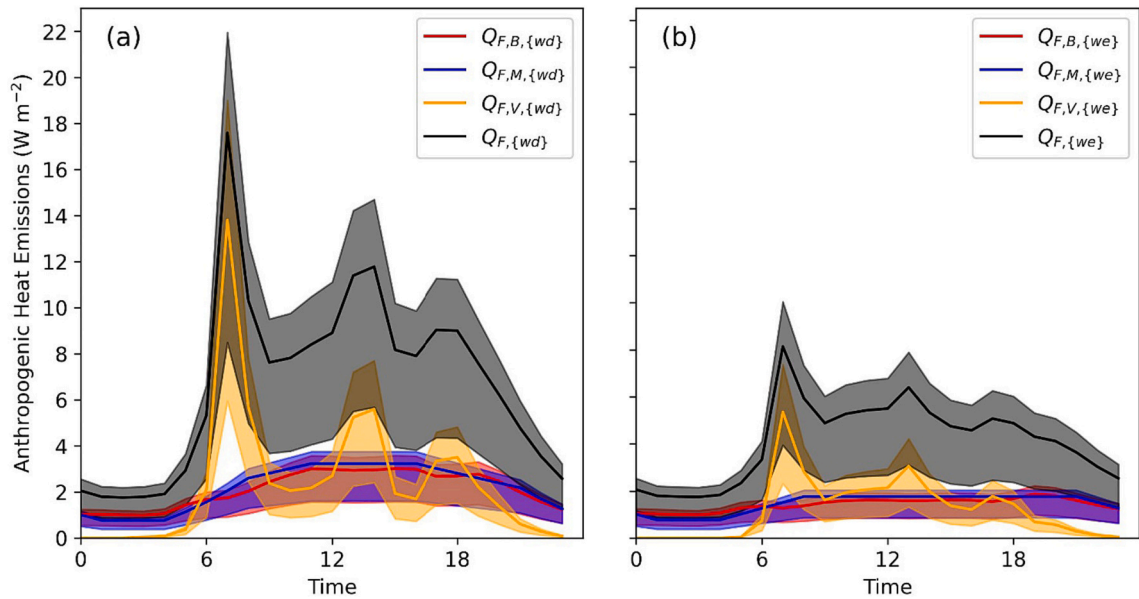
Fig. 5. Diurnal variation (mean: line, interquartile range: shading) of Q_F and its components for grid cells within Colombo on (a) workdays (*wd*) and (b) non-workdays (*we*).

density in the morning (Fig. 4a).

The maximum $Q_{F,V,\{wd\}}$ (13.8 W m^{-2}) occurs at 07:00, and is 5.8 times larger than the *wd* mean (Fig. 5c, Table 4). This morning peak is associated with work and school related trips (JICA (2014), their Fig. 3.1.23). A second, smaller peak at 14:00 is associated with the collection of school pupils (JICA (2014), their Fig. 3.1.23). The third peak at 18:00 is smaller (Fig. 5c), and is associated with workers commuting home (JICA (2014), their Fig. 3.1.23). This three-peaked $Q_{F,V}$ diurnal profile (Fig. 5c) differs from other cities where vehicle counts are used with two approximately equal sized peaks in the morning and evening (Sailor and Lu, 2004; Allen et al., 2011; Quah and Roth, 2012; CAMS, 2019).

The diurnal range for $Q_{F,B,\{wd\}}$ (1.0 → 3.0 W m^{-2}) is much smaller than for $Q_{F,M}$ and $Q_{F,V}$. The Colombo $Q_{F,\{wd\}}$ diurnal range ratio of ~10 (1.8 W m^{-2} (02:00) → 17.6 W m^{-2} (07:00)) is much larger than the global mean diurnal range ratio of ~5 (0.7 → 3.6 W m^{-2}) estimated by Allen et al. (2011), or in United States cities of ~3–4 predicted by Sailor and Lu (2004). In the daytime on workdays, Colombo's AHEs would be underestimated by as much as 10.9 W m^{-2} if assumed constant through time. Non-workdays have a smaller diurnal range (1.7 W m^{-2} (03:00) → 8.1 W m^{-2} (07:00)).

4.2. Spatial variations: local climate zone (LCZ)

The spatial variation of LCZs (Table 4, Fig. 1d) is linked to building: packing (compact and open), height (high-, medium-, and low-rise), thermal properties (lightweight), and extent (large) (Stewart and Oke, 2012).

With little variation in plan area fraction of road (f_{rd}) (Fig. 3c) between LCZs the $Q_{F,V}$ is very similar (≈ 2 W m^{-2} Table 4). Overall, the largest Q_F are associated with open – high-rise (LCZ4 = 13.2 W m^{-2}) and compact – high-rise (LCZ1 = 10.4 W m^{-2}). The LCZ4 Q_F is larger than LCZ1 despite being less dense because of the building volume. This is used to downscale the divisional secretariat population density (Section 3.3) and in-turn the population density is used to downscale the Colombo (N, S, E, and W) electricity consumption data. Hence, both $Q_{F,M}$ and $Q_{F,B}$ are related to building height (Table 4); resulting in Q_F being smaller with decreasing building height within LCZs 1 to 3 and LCZs 4 to 6.

The W region of Colombo (Fig. 6) has most of the tall buildings (Fig. 3a) and the largest mean electricity consumption (1.5 W m^{-2}, Table 4). It also has the largest total building volume per area (4.45 m, Table 4). LCZs 1 and 4 have high $Q_{F,B}$ (Table 4) and are common in the W region, but $Q_{F,B}/Q_{F,M}$ is lowest there (LCZ4 = 0.81, LCZ1 = 0.89) because electricity consumption per capita is lowest in the W region. This ratio is highest for LCZ6 (1.06, Table 4).

4.3. Spatial variations: four neighbourhoods

We explore in more detail four (~ 1 km^2 scale) Colombo "neighbourhoods" (Fig. 6, magenta) with distinct and different characteristics (Table 5).

The "dense", northernmost, neighbourhood has a high proportion of commercial and business land use classes (JICA (2014), their Fig. 2.2.3). Of the four, this neighbourhood has the highest density of people ($\rho_{noc} = 337$ capita ha^{-1}) and the largest plan area fraction of buildings ($f_{bld} = 0.64$). The "tall" neighbourhood in the middle-west has many of the tallest buildings (seven of the 100 m $\times$ 100 m
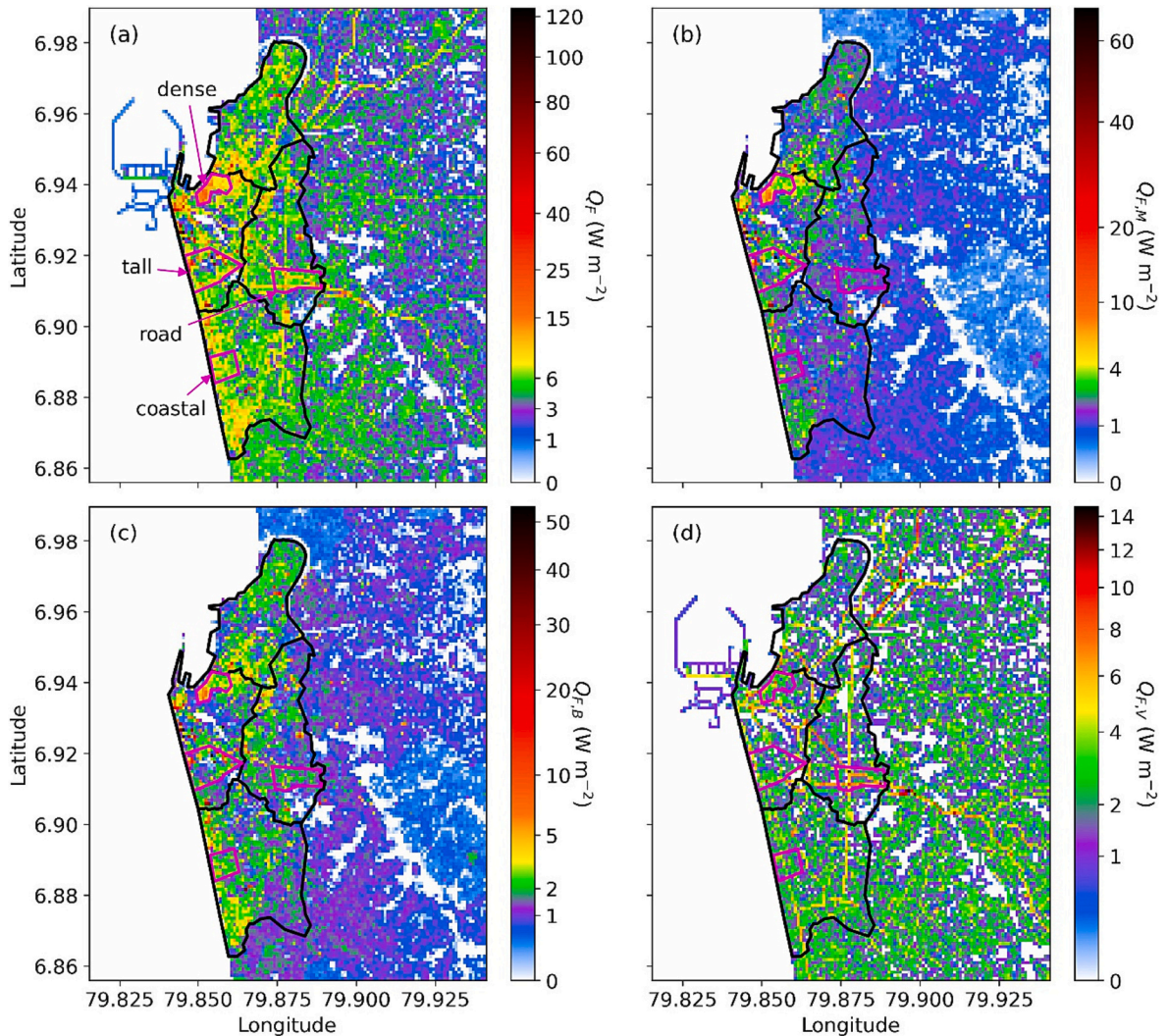
Fig. 6. Colombo (with its four electricity consumption regions; N, S, E, and W, black; and four neighbourhoods (dense, tall, coastal, and road, magenta, Table 5)) and surrounding (100 m × 100 m resolution) 2020 annual-average anthropogenic heat flux (colour, logarithmic scale): (a) total, and related to (b) buildings, (c) metabolism, and (d) motorised transport. (For interpretation of the references to colour in this figure legend, the reader is referred to the web version of this article.)

Table 5

Characteristics of four neighbourhoods (Fig. 6) in two divisional secretariats (a,b) in Colombo: plan area fraction of buildings (f_{bld}) and roads (f_{rd}), mean building height (h), population density on workdays (ρ_{wd}), and the anthropogenic heat fluxes (MD – median, IQR – interquartile range) for 2020.

Neighbourhoods	Land use	f_{bld}	f_{rd}	ρ_{wd} (capita ha^{-1})	h (m)	Flux (W m^{-2})		
						Mean	MD	IQR
(a) Colombo								
Dense (North)	very-dense, large commercial	0.64	0.08	555	9.0	10.4	10.0	4.6
Tall (Middle-West)	many tall buildings	0.39	0.06	532	15.7	8.9	6.4	4.5
Road (Middle-East)	largely residential, main road artery	0.43	0.10	233	7.1	6.8	6.0	3.3
(b) *Thimbirigasyaya*								
Coastal (South)	largely residential, coast	0.48	0.07	294	7.9	6.5	6.5	2.3

grid cells having $h > 50$ m) and the tallest neighbourhood mean building height ($h = 16.1$ m). The middle-east neighbourhood contains a major arterial "road" but mainly residential land use. This neighbourhood has the largest plan area fraction of road ($f_{rd} = 0.10$) and lowest population density ($\rho_{noc} = 108$ capita ha^{-1}). The largely residential neighbourhood to the south is "coastal", unlike the inland

middle-east neighbourhood. It has the second largest plan area fraction of buildings ($f_{bld} = 0.48$), but with a short mean building height ($h = 7.9$ m) and a residential population density of 136 capita ha^{-1}.

To compare the 2020 annual average Q_F variability in the neighbourhoods, we use probability density functions (PDFs) (each integrates to 1, Fig. 7). Spatial averages and PDFs include 0 W m^{-2} grid cells. The dense, high population density neighbourhood (Table 5), located in the highest (W) electricity consumption region has the largest mean Q_F ($= 10.4$ W m^{-2}). The maximum individual grid-cell values are in the range 18–20 W m^{-2}. Whereas the tall neighbourhood has several grid-cells with $Q_F > 25$ W m^{-2}, with the extreme being 114 W m^{-2}, despite having a smaller spatial mean (8.9 W m^{-2}). This is linked to the neighbourhood also having a lake, several parks, and several low-rise, low population density, residential areas. Hence, the distribution is more positively skewed for the tall (Fig. 9b) neighbourhood than the dense (Fig. 9a) neighbourhood. In the tall neighbourhood, 4–6 W m^{-2} and 6–8 W m^{-2} are equally common, while in the dense neighbourhood 10–12 W m^{-2} is most common.

The largely residential coast and road neighbourhoods have smaller mean Q_F values (6.5 and 6.8 W m^{-2}, respectively), with all grid cells having values <16 W m^{-2} (Fig. 7c,d). They have smaller $Q_{F,B}$ and $Q_{F,M}$ values (cf. tall and dense), and $Q_{F,V}$ makes a 51% contribution to Q_F in the road neighbourhood (cf. 27%, 23%, and 35% in dense, tall, and coast neighbourhoods, respectively).

The Colombo (Fig. 6) median Q_F is 5.4 W m^{-2}, while the mean is 5.9 W m^{-2}. Thus, Q_F is not normally distributed, with extremes impacting the mean. The 90, 99 and 99.5 percentiles are 9.3, 20.9, and 32.9 W m^{-2}, respectively. Hence, the tall neighbourhood peak values are amongst the largest in Colombo. The AH4GUC (Varquez et al., 2021) Colombo mean and median are 6.1 and 3.3 W m^{-2} (Table 4), respectively, suggesting the AH4GUC values are less normally distributed, with a higher proportion of small values. Both models use population density for downscaling Q_F, but an important difference is the use of road fraction in the downscaling of transport emissions in this study. Also, the population density in this study is based on divisional secretariat population data downscaled using 100 m gridded building footprint data, whereas AH4GUC population density is based on the 1 km resolution LandScan™ population dataset (Dobson et al., 2000) with 1 km resolution VIIRS Nighttime Lights (Elvidge et al., 2017) correction.

Overall, there are larger intra-neighbourhood variations in Q_F (Fig. 7) than inter-neighbourhood differences (Table 5), with the smallest Q_F neighbourhood value being more than half the largest (Table 5). Grid length impacts Q_F spatial heterogeneity (Lindberg et al., 2013). Large Q_F values in 100 m grid cells are often surrounded by much lower values. This is problematic for surface energy
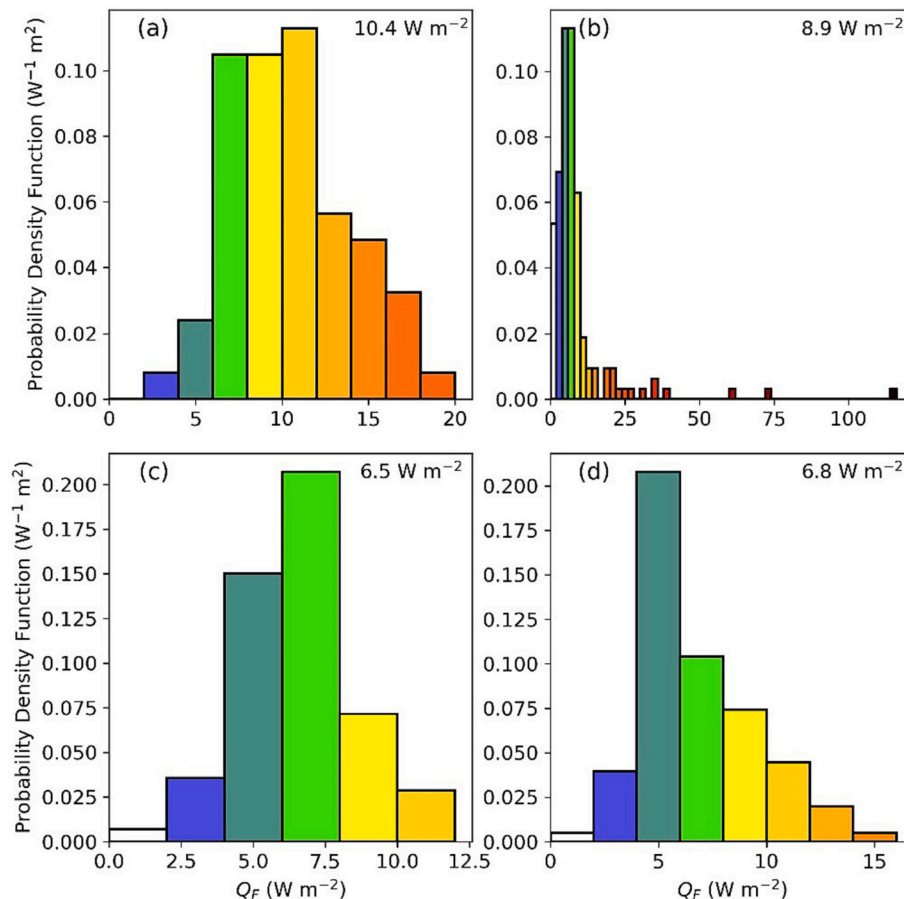

Fig. 7. Probability density functions (2 W m^{-2} bins, colours correspond to Fig. 6a colour bar) for grid cells (100 m × 100 m) in four neighbourhoods (Fig. 6, Table 5) and mean of Q_F (top right corner) for 2020: (a) dense, (b) tall, (c) coastal, and (d) road.

balance models that do not represent horizontal advection (e.g. offline simulations uncoupled from a 3-D atmospheric model) or without spatial smoothing. Grid cells with large Q_F values can cause unrealistically warm air temperatures compared to adjacent grid cells, if Q_F is not diluted by advection. This could be addressed by smoothing using a gaussian or linear filter (e.g. O(0.5–1 km)) to reduce the highest spatial variations (i.e. an intentional underestimate). This highlights the advantage of using a vertically distributed canopy model, as O(100 m) grid cells can be used to capture the spatial variation in Q_F, whilst also representing horizontal advection within the canopy.

The maximum (2020 annual average) Q_F in one grid cell in Colombo is 124 W m^{-2}, which is much larger than the maximum AH4GUC Q_F (2010 annual average) Colombo single grid cell value of 31.7 W m^{-2}. This is probably largely linked to the larger areal extent of the 1 km AH4GUC grid cell (cf. our study 100 m).

4.4. Spatial and temporal variations: influence of coarse graining

The impact of spatial scale (grid-length resolution) is known to have a significant impact on the Q_F intensity. Many individual city studies have used 100 m resolution (e.g. Grimmond, 1992; Kłysik, 1996; Ichinose et al., 1999; Pigeon et al., 2007; Quah and Roth, 2012) but when the spatial coverage is global the grid length is much larger (e.g. 0.5° x 0.5°, Flanner, 2009; 2.5′ x 2.5′, Allen et al., 2011). Lindberg et al. (2013) designed their global model to be able to change spatial resolution and demonstrate the impacts (as well as providing the data at many different grid-resolutions). For Greater London they demonstrate that spatial coarsening results in a large drop in maximum flux (e.g., dropping from ~68 W m^{-2} (30″ resolution) to ~35 W m^{-2} (10′ resolution)), and collapse of both the slope of decreasing spatial mean and city-wide mean (Lindberg et al., 2013, their Fig. 8).

In our study area, the 2020 annual average Q_F after coarse graining the 100 m grid length to 200 m, 400 m (etc.) up to 6.4 km grid length shows similar influences of spatial resolution on Q_F spatial variability. For grid-cells within the CMC (Fig. 8a), the maximum value falls from 124 W m^{-2} (100 m resolution) to 29 W m^{-2} (200 m resolution) to 10 W m^{-2} (1.6 km), and plateaus at ~3.2 km resolution where it approximately equals the CMC spatial mean. The spatial maximum decreases less rapidly with increasing grid length. The difference between the 95th and 5th percentiles is 10.0, 5.0, and 1.7 W m^{-2} at 100 m, 800 m, and 3.2 km grid lengths, respectively. Therefore, the horizontal heterogeneity in Q_F falls rapidly from the hectometre to the kilometre scale. Gabey et al. (2019) found Q_F hot spots are missed when Q_F is coarse grained from 500 m to 5 km grid length. Our results demonstrate, as expected, there is further Q_F detail at sub-500 m grid length. Moving from kilometre scale to sub-kilometre scale NWP and climate modelling will have a large influence on the need for information about Q_F spatial variability (if represented at commensurate scale), and sub-km simulations can therefore be expected to demonstrate more fine-scale detail on the near-surface urban climate.

Spatial coarse graining by day type (workdays (wd) and non-workdays (we)), allows hourly differences between the 95th and 5th percentiles (q_{95}-q_5) of Q_F within the CMC to be calculated (Fig. 8b). The wd maximum is 38.7, 14.2, and 4.4 W m^{-2} at 100 m, 800 m, and 3.2 km grid lengths, respectively, and occurs at 07:00 which coincides with maximum daily Q_F (Fig. 5). Scaling by the CMC mean
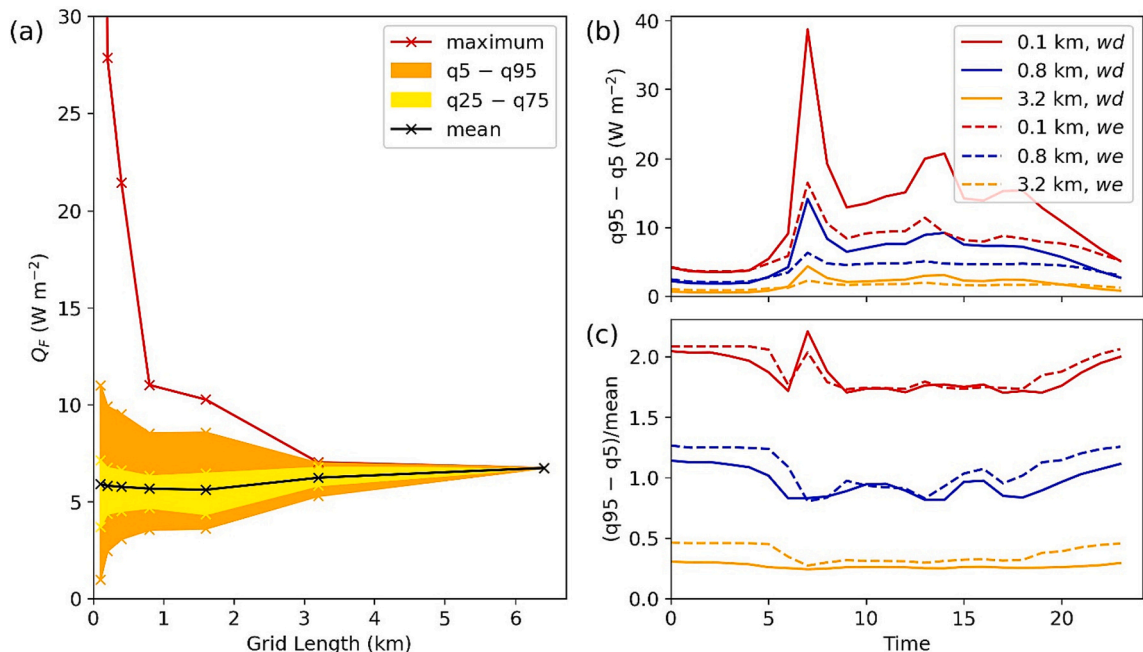

Fig. 8. Impact of grid-cell spatial resolution calculated in CMC from 2020 annual average Q_F data: (a) maximum, mean, and percentiles. Note overall mean Q_F values vary slightly with resolution because the CMC region is modified by the exact grid points falling within it. (b) Diurnal variability of 95th to 5th percentiles (q_{95}-q_5) range for workdays (wd) and non-workdays (we). (c) As (b), except normalised.

Table 6

Current (2020) and future (2035) conditions modelled for projections (P) 1 to 5. The change in population (Δ_{Pop}) and trips (Δ_{Trip}) are an increase over the current. Local climate zone (LCZ, Table 4, NU – non-urban) cover. Trips have the following modes: non-motorised (NM, e.g. walking, cycling), train (Tr), motorbike (MB), and three-wheeler (3 W). The projected 2035 annual average AHEs by component for Colombo.

Code	Δ_{Pop} (%)	LCZ Cover (%)											Δ_{Trip} (%)	Trip Share (%)						2035 Q_F (W m^{-2})			
P#		1	2	3	4	5	6	7	8	9	10	NU		NM	Bus	Tr	Car	MB	3 W	$Q_{F,M}$	$Q_{F,B}$	$Q_{F,V}$	Q_F
2020	0	6	27	31	3	2	3	1	17	0	2	8	0	21	38	3	11	14	13	1.98	1.91	2.05	5.94
1	24	6	27	31	3	2	3	1	17	0	2	8	25	21	38	3	11	14	13	2.46	2.37	2.56	7.39
2	68	69	0	23	0	0	0	0	0	0	0	8	25	21	38	3	11	14	13	3.32	2.99	2.56	8.87
3	68	69	0	23	0	0	0	0	0	0	0	8	25	17	32	2	32	8	7	3.32	2.99	3.23	9.54
4	68	69	0	23	0	0	0	0	0	0	0	8	25	17	49	4	9	11	10	3.32	2.99	2.20	8.51
5	24	45	0	47	0	0	0	0	0	0	0	8	25	21	38	3	11	14	13	2.46	2.49	2.56	7.51

hourly Q_F gives almost constant diurnal profiles at all grid lengths (Fig. 8c). Therefore, although the magnitude of spatial differences in Q_F are greatest at 07:00, the spatial heterogeneity does not change much throughout the day. Comparing *wd* and *we* temporal profiles by grid resolution (Fig. 8c), shows the spatial heterogeneity to be similar for *wd* and *we*. One would expect large Q_F spatial heterogeneity (i.e. normalised) diurnal variation if the temporal behaviour of Q_F varies significantly by location. The lack of Q_F spatial heterogeneity diurnal variation is explained by the largest overall Q_F being linked with $Q_{F,B}$ and $Q_{F,M}$ values (Fig. 6), which have similar diurnal profiles (Fig. 5).

4.5. 2035 Projections

It is critical to know not only about current conditions (i.e. 2020, Section 4.1-4.4), but also future conditions as any building being planned now will experience and impact those conditions. To address this, five projections for Colombo in 2035 are made based on different population, land cover, and transport scenarios (Table 6) as this is a period with local published plans. The warming climate is not represented in the projections, since space heating and cooling are the temperature sensitive contributors to Q_F, but currently are a small fraction of Q_F in Colombo (Table 4).

Projection 1 (P1, Table 6) assumes an increase in population (0.613 to 0.761 million) based on United Nations (UN), 2019 estimates and that the inter-LCZ proportions remain the same. Hence, the population increase is assumed to be met without any change in buildings. P2 − P4, assume a population of 1.028 million, the non-urban (NU) LCZ cover in Colombo (i.e. within the CMC, Fig. 1c) remains 8% (Table 6) but LCZ1 becomes 69% and LCZ3 23% (Table 6) based on the Colombo Core Area Development Plan (CCADP) scenario for 2035 (Rathnayake et al., 2020). The population increases are met by an increase in total building volume, while the building volume per person remains constant. As a 68% increase in population in 15 years is very large, P5 uses the smaller UN predicted population, with smaller building volume increases occurring in LCZ1 and LCZ3 so that the building volume per person remains constant (Table 6).

Increased transport needs are projected to result in an increase from 2.4 million trips per day to 3 million per day for P1 − P5 (JICA (2014), their Fig. 5.2.1). The increase is mainly associated with population growth in the suburbs and a resulting increase in Colombo commuters (JICA (2014), their Section 5.2.1). For P1, P2, and P5 the mode fractions are assumed to remain unchanged. With increases in household income, it is expected more trips may occur using private transport unless public transport infrastructure improves (JICA (2014), their Section 5.2.1). P3 assumes car-oriented transport with extra trips met by a 260% increase in car trips, while P4 assumes public transport meets the needs via a 53% increase in bus and train trips. The car-oriented transport scenario (P3) assumes private car ownership becomes widely affordable and that there is space to park the cars.

The change in fluxes involves scaling the current $Q_{F,M}$ by the population increase. Similarly, $Q_{F,V}$ values are scaled by the change in number of trips per mode. For buildings, in P1 $Q_{F,B}$ is scaled by the population increase; while P2 − P5 also account for the LCZ specific values with the change in LCZ weightings.

The simulated projections result in a 24% to 61% increase in mean Q_F. P2 − P4 are the largest (Table 6) with increases (cf. 2020) of 49%, 61%, and 43%, respectively. These are linked to the largest population density CCADP land cover projections (Table 6), hence having large $Q_{F,B}$ and $Q_{F,M}$. The CCADP land cover assumes a large proportion of LCZ1, with high $Q_{F,B}$ linked to the highest (W) electricity consumption region (Table 4).

Of the CCADP land cover projections, the car-oriented transport scenario (P3) has the highest Q_F, with a $Q_{F,V}$ increase of 1.2 W m^{-2} (58%) whereas the public transport (P4) $Q_{F,V}$ increases by only 0.2 W m^{-2} (7%) (Table 6). Hence, the AHE impacts can be reduced by encouraging public over private transport trip choices ($\approx$ 1 W m^{-2} less).

P1 and P5 have the smallest Q_F increases (24% and 26%, respectively), because of the use of lower UN predicted population increase than the CCADP LCZ based population estimates (P2 − P4). Lindberg et al.'s (2013) investigation of changes in Q_F between 1995 and 2015 for a region including many European cities using the LUCY model, found with a population decrease of 3.6% in the period whilst keeping other variables constant, that the expected decrease in Q_F was simulated to be only 1%. The Q_F values were relatively insensitive to large changes in traffic volume. This contrasts with Colombo where $Q_{F,M}$ and $Q_{F,V}$ contribute a large proportion to Q_F. With large projected increases in population density and trips, the $Q_{F,M}$ and $Q_{F,V}$ increase Q_F by between 8 and 23% and 3–20%, respectively.

Lindberg et al. (2013) estimate that between 1995 and 2015 European city Q_F increases are 10–12% from $Q_{F,B}$. Here we assume $Q_{F,B}$ increases are either in proportion to population density (P1, P5) or in proportion to current LCZ1 and LCZ3 $Q_{F,B}$ values (P2 − P4). The projected $Q_{F,B}$ increases result in Q_F increases in the range of 8–18% (Table 6). Large uncertainty in $Q_{F,B}$ estimates for Colombo arise from several inter-related factors, such as the future cost of electricity, development of the energy grid, growth in gross domestic product, and perhaps most importantly whether AC becomes more widely adopted in future building design. There is no consideration in this study of the implications of the global energy crisis (Economist, 2022a), the implications of the current economic situation in Sri Lanka (Economist, 2022b), or changes in nutrition. For different climate change scenarios Lindberg et al. (2013) found Q_F to be most sensitive to changes in temperature. This is unlikely the case for Colombo since AC electricity consumption is currently small there. However, given the uncertainty in AC usage between 2020 and 2035 and beyond, sensitivity of Q_F to climate change under different AC scenarios is worthy of future study.

5. Conclusions

Anthropogenic heat emissions (AHEs) are estimated for the lower-middle income, low-latitude city of Colombo and its surroundings. Unlike previous AHE studies of this type of city, we derive high-resolution land cover and morphology data, and combine

with spatially and temporally detailed transport and electricity consumption data. This allows spatial variation of AHE components to be obtained at 100 m (grid cell), and aggregation to different neighbourhoods and the whole city scale. The temporal variability in AHE components considers diurnal differences by day type (work/non-work) and future city conditions (in 2035).

The city wide mean anthropogenic heat flux for 2020 is 5.9 W m^{-2}, with the contributions to total emissions being transport (35%), metabolic (33%) and building (32%). The building emissions are a smaller proportion than reported for mid-latitude and high-income, low-latitude cities, attributed to little heavy industry, minimal need for winter-time space heating, and very little use of air conditioning. The latter is despite Colombo often experiencing air temperatures >30 °C. This low $Q_{F,B}$ value results in the overall mean Q_F value being smaller than many mid-latitude cities.

However, Colombo has large spatial heterogeneity between 100 m grid cells. The largest values are attributed to areas with high-rise buildings occupying large fractions of a grid cell (maximum = 124 W m^{-2}). With high population densities, there are large AHEs from both metabolic and electrical appliance usage. Four contrasting kilometre-scale neighbourhoods (with dense buildings, tall buildings, residential buildings with a major road and residential buildings along the coast) have mean Q_F between 6.5 and 10.4 W m^{-2}. This demonstrates that AHEs become more homogeneous at the neighbourhood scale in Colombo.

Colombo mean Q_F for workdays (6.7 W m^{-2}) are larger than non-workdays (4.1 W m^{-2}). There are large diurnal variations with minimum on workdays of 1.8 W m^{-2} (02,00) and peak of 17.6 W m^{-2} (07,00). Non-workdays have the same minimum at a similar time (03,00) but a much smaller peak (8.1 W m^{-2} at 07,00). The workday peak is largely from work and school trips related transport emissions. Two other smaller peaks (14,00 and 18,00) are associated with school pupils going home and workers commuting home (respectively). The three peak diurnal profile is not evident in cities when school collection overlaps with the home commute. AHEs are larger during the day than at night because of more transport emissions, higher electricity consumption, and larger metabolic emissions from both greater human activity and population density.

Spatial resolution or coarse graining the grid-cell resolution causes the maximum Q_F to fall rapidly from 124 W m^{-2} (100 m resolution) to 10 W m^{-2} (1.6 km resolution), with it approximately equalling the CMC region mean at 3.2 km resolution. Horizontal heterogeneity in Q_F falls rapidly from the hectometre to the kilometre scale. Spatial heterogeneity in Q_F changes little between day types (non-work, work day) and by hour of day. This is because the largest spatial variations in Q_F are associated with $Q_{F,B}$ and $Q_{F,M}$ heterogeneity, and these have similar diurnal profiles.

Anthropogenic heat flux projections for 2035 vary between 7.5 and 9.5 W m^{-2} (i.e. 24% and 61% increases from the 2020 value, respectively). Population density is an important driver of these AHE increases, again linked to metabolic emissions, number of trips made within the city, and amount of electricity consumed. If increases in trips are met by public rather than private transport, this would result in a 1 W m^{-2} lower mean flux across the whole city.

These results have application to future building design. Densely built-up neighbourhoods tend to have large Q_F and coincide with high population density. Also, individual tall buildings may have very large AHEs, with the heat in their wakes influencing the stability of the downstream boundary layer and neighbourhood conditions, particularly in calm nights. Building design must account for neighbourhood specific meteorological factors such as Q_F, shading, and ventilation potential, to alleviate anthropogenically exacerbated extreme heat conditions. The simulated Q_F values provide indicative values for other lower-middle income, low-latitude cities, where data are not available. Future studies could incorporate city-level residential photovoltaic energy generation data and consider AC consumption scenarios.

Author statement

All authors have seen and approved the final version of the manuscript being submitted. They warrant that the article is the author's original work, hasn't received prior publication, and isn't under consideration for publication elsewhere.

CRediT authorship contribution statement

Lewis Blunn: Conceptualization, Data curation, Formal analysis, Investigation, Methodology, Visualization, Writing – original draft, Writing – review & editing. **Xiaoxiong Xie:** Data curation, Formal analysis, Investigation, Methodology, Software, Visualization, Writing – original draft, Writing – review & editing. **Sue Grimmond:** Conceptualization, Funding acquisition, Methodology, Project administration, Resources, Supervision, Writing – original draft, Writing – review & editing. **Zhiwen Luo:** Conceptualization, Funding acquisition, Investigation, Methodology, Project administration, Resources, Supervision, Writing – review & editing. **Ting Sun:** Resources, Writing – review & editing. **Narein Perera:** Funding acquisition, Investigation, Project administration, Resources, Writing – review & editing. **Rangajeewa Ratnayake:** Funding acquisition, Investigation, Project administration, Resources, Writing – review & editing. **Rohinton Emmanuel:** Funding acquisition, Investigation, Project administration, Resources, Writing – review & editing.

Declaration of competing interest

The authors declare the following financial interests/personal relationships which may be considered as potential competing interests: Luo, Grimmond, Emmanuel reports financial support was provided by UK Research and Innovation. Grimmond reports financial support was provided by European Commission. Grimmond on editorial board.

Data availability

Data will be made available on request.

Acknowledgements

Appendix A. Supplementary data

Supplementary data to this article can be found online at https://doi.org/10.1016/j.uclim.2024.101828.

References

Adunola, A.O., 2014. Evaluation of urban residential thermal comfort in relation to indoor and outdoor air temperatures in Ibadan, Nigeria. Build. Environ. 75, 190–205.

Allen, L., Lindberg, F., Grimmond, C., 2011. Global to city scale urban anthropogenic heat flux: model and variability. Int. J. Climatol. 31, 1990–2005.

Ao, X., Grimmond, C.S., Ward, H.C., Gabey, A.M., Tan, J., Yang, X.Q., Liu, D., Zhi, X., Liu, H., Zhang, N., 2018. Evaluation of the Surface Urban Energy and Water balance Scheme (SUEWS) at a dense urban site in Shanghai: Sensitivity to anthropogenic heat and irrigation. J. Hydrometeorol. 19, 1983–2005.

Beck, H.E., Zimmermann, N.E., McVicar, T.R., Vergopolan, N., Berg, A., Wood, E.F., 2018. Present and future Koppen-Geiger climate classification maps at 1-km resolution. Sci. Data 5, 1–12.

Blunn, L., Xie, X., Grimmond, S., Luo, Z., Sun, T., Perera, N., Ratnayake, R., Emmanuel, R., 2022. Spatial and temporal variation of anthropogenic heat emissions in Colombo, Sri Lanka - Data files. https://doi.org/10.5281/zenodo.7245097.

Bohnenstengel, S., Hamilton, I., Davies, M., Belcher, S., 2014. Impact of anthropogenic heat emissions on London's temperatures. Q. J. R. Meteorol. Soc. 140, 687–698.

Copernicus Atmosphere Monitoring Service (CAMS), 2019. D81.6.2.1: report on emission temporal profiles for the global and regional scales. URL: https://atmosphere.copernicus.eu/sites/default/files/2019-11/27_CAMS81_2017SC1_D81.6.2.1-201902_v1_APPROVED_Ver1.pdf.

Capel-Timms, I., Smith, S.T., Sun, T., Grimmond, S., 2020. Dynamic anthropogenic activities impacting heat emissions (DASH v1.0): development and evaluation. Geosci. Model Dev. 13, 4891–4924.

Coffel, E.D., Horton, R.M., De Sherbinin, A., 2017. Temperature and humidity based projections of a rapid rise in global heat stress exposure during the 21st century. Environ. Res. Lett. 13, 014001.

Congedo, L., 2021. Semi-automatic classification plugin: a Python tool for the download and processing of remote sensing images in QGIS. J. Open Source Softw. 6, 3172.

Demuzere, M., Kittner, J., Bechtel, B., 2021. LCZ Generator: a web application to create local climate zone maps. Front. Environ. Sci. 9.

Dept. of Census and Statistics, 2012. Census of Population and Housing, 2012v. URL: http://www.statistics.gov.lk/pophousat/cph2011/pages/activities/reports/finalreport/finalreporte.pdf (accessed 10.03.22).

Dimitroulopoulou, C., 2012. Ventilation in European dwellings: a review. Build. Environ. 47, 109–125.

Dobson, J.E., Coleman, P.R., Durfee, R.C., Worley, B.A., 2000. LandScan: a global population database for estimating populations at risk. Photogramm. Eng. Remote. Sens. 66, 849–857.

Dong, Y., Varquez, A., Kanda, M., 2017. Global anthropogenic heat flux database with high spatial resolution. Atmos. Environ. 150, 276–294.

Economist, 2022a. How to Fix the world's Energy Emergency without Wrecking the Environment. URL: https://www.economist.com/leaders/2022/06/23/how-to-fix-the-worlds-energy-emergency-without-wrecking-the-environment.

Economist, 2022b. Why is Sri Lanka in turmoil? URL: https://www.economist.com/the-economist-explains/2022/07/19/why-is-sri-lanka-in-turmoil (accessed 09.28.2022).

Elvidge, C.D., Baugh, K., Zhizhin, M., Hsu, F.C., Ghosh, T., 2017. VIIRS night-time lights. Int. J. Remote Sens. 38, 5860–5879.

Emmanuel, R., Johansson, E., 2006. Influence of urban morphology and sea breeze on hot humid microclimate: the case of Colombo, Sri Lanka. Clim. Res. 30, 189–200.

European Commission (EC), 2017. Study on the Implementation of Article 7(3) of the "Directive on the Deployment of Alternative Fuels Infrastructure" – Fuel Price Comparison. URL: https://op.europa.eu/en/publication-detail/-/publication/d0d5be35-1a94-11e7-808e-01aa75ed71a1/language-en.

European Space Agency (ESA), 2018. Sentinel-2 products specification document. URL: https://sentinel.esa.int/documents/247904/685211/sentinel-2-products-specification-document.

Flanner, M.G., 2009. Integrating anthropogenic heat flux with global climate models. Geophys. Res. Lett. 36, L02801.

Food and Agriculture Organization (FAO) of the United Nations, 2012. World agriculture towards 2030/2050. URL: https://www.fao.org/3/ap106e/ap106e.pdf (accessed 12.03.22).

Gabey, A., Grimmond, C., Capel-Timms, I., 2019. Anthropogenic heat flux: advisable spatial resolutions when input data are scarce. Theor. Appl. Climatol. 135, 791–807.

Google, 2022. Google Earth Imagery. URL: https://www.google.co.uk/maps.

Grimmond, C., 1992. The suburban energy balance: methodological considerations and results for a mid-latitude west coast city under winter and spring conditions. Int. J. Climatol. 12, 481–497.

Hamilton, I.G., Davies, M., Steadman, P., Stone, A., Ridley, I., Evans, S., 2009. The significance of the anthropogenic heat emissions of London's buildings: a comparison against captured shortwave solar radiation. Build. Environ. 44, 807–817.

Hinkel, K.M., Nelson, F.E., Klene, A.E., Bell, J.H., 2003. The urban heat island in winter at Barrow, Alaska. Int. J. Climatol. 23, 1889–1905.

Ichinose, T., Shimodozono, K., Hanaki, K., 1999. Impact of anthropogenic heat on urban climate in Tokyo. Atmos. Environ. 33, 3897–3909.

Japan International Cooperation Agency (JICA), 2014. Urban Transportation System Development Project for Colombo Metropolitan Region and Suburbs (CoMTrans), Final Report. URL: https://openjicareport.jica.go.jp/pdf/12176665.pdf.

Järvi, L., Grimmond, C., Christen, A., 2011. The surface urban energy and water balance scheme (SUEWS): evaluation in Los Angeles and Vancouver. J. Hydrol. 411, 219–237.

Jayatissa, R., Marasingha, W., 2022. Nutrition Status and Gaps in the Diet of Sri Lankans during the Pre-Economic Crisis Period (from September to December 2021). URL: http://www.mri.gov.lk/wp-content/uploads/2022/09/Diet-adequacy_Final-Report.pdf.

Jayawardena, R., Thennakoon, S., Byrne, N., Soares, M., Katulanda, P., Hills, A., 2014. Energy and nutrient intakes among Sri Lankan adults. Int. Arch. Med. 7, 1–11.

Jayaweera, N., Jayasinghe, C.L., Weerasinghe, S.N., 2018. Local factors affecting the spatial diffusion of residential photovoltaic adoption in Sri Lanka. Energy Policy 119, 59–67.

Kłysik, K., 1996. Spatial and seasonal distribution of anthropogenic heat emissions in Lodz, Poland. Atmos. Environ. 30, 3397–3404.

Kotthaus, S., Grimmond, C., 2012. Identification of micro-scale anthropogenic CO2, heat and moisture sources – processing eddy covariance fluxes for a dense urban environment. Atmos. Environ. 57, 301–316.

Leroyer, S., Bélair, S., Souvanlasy, V., Vallée, M., Pellerin, S., Sills, D., 2022. Summertime assessment of an urban-scale numerical weather prediction system for Toronto. Atmosphere 13, 1030.

Lindberg, F., Grimmond, C.S.B., Yogeswaran, N., Kotthaus, S., Allen, L., 2013. Impact of city changes and weather on anthropogenic heat flux in Europe 1995–2015. Urban Clim. 4, 1–15.

Mason, J.B., 2002. Lessons on nutrition of displaced people. J. Nutr. 132, 2096S–2103S.

Ming, Y., Liu, Y., Liu, X., 2021. Spatial pattern of anthropogenic heat flux in monocentric and polycentric cities: the case of Chengdu and Chongqing. Sustain. Cities Soc. 78, 103628.

Ministry of Transport and Civil Aviation (MTCA), 2018. Progress Report – 2018. URL: https://www.transport.gov.lk/web/images/pdf/progress_english_2018.pdf.

National Centers for Environmental Information (NOAA), 2001. Global Surface Hourly – Station 43466099999. URL: https://www.ncei.noaa.gov/access/search/data-search/global-hourly.

OpenStreetMap contributors, 2021. Planet dump retrieved from https://planet.osm.org [WWW Document]. URL: https://www.openstreetmap.org (accessed: 08.31.22).

Pallegedara, A., Mottaleb, K.A., Rahut, D.B., 2021. Exploring choice and expenditure on energy for domestic works by the Sri Lankan households: implications for policy. Energy 222, 119899.

Perera, N., 2021. WUDAPT Level 0 training data for Colombo. URL: https://lcz-generator.rub.de/factsheets/50996c3981a5b84e4058dcc23578a7ddc9011a3a/50996c3981a5b84e4058dcc23578a7ddc9011a3a_factsheet.html (accessed 09.15.21).

Perera, N.G.R., Emmanuel, R., 2018. A "Local Climate Zone" based approach to urban planning in Colombo, Sri Lanka. Urban Clim. 23, 188–203.

Pigeon, G., Legain, D., Durand, P., Masson, V., 2007. Anthropogenic heat release in an old European agglomeration (Toulouse, France). Int. J. Climatol. 27, 1969–1981.

QGIS Development Team, 2022. QGIS Geographic Information System. URL: https://www.qgis.org.

Quah, A.K., Roth, M., 2012. Diurnal and weekly variation of anthropogenic heat emissions in a tropical city, Singapore. Atmos. Environ. 46, 92–103.

Ramsay, E.E., Fleming, G.M., Faber, P.A., Barker, S.F., Sweeney, R., Taruc, R.R., Chown, S.L., Duffy, G.A., 2021. Chronic heat stress in tropical urban informal settlements. Iscience 24, 103248.

Rathnayake, N.U., Perera, N.G.R., Emmanuel, M.P.R., 2020. Anthropogenic heat implications of Colombo Core Area Development Plan. IOP Conf. Ser. Earth Environ. Sci. 471, 012002.

Ronda, R.J., Steeneveld, G.J., Heusinkveld, B.G., Attema, J.J., Holtslag, A.A.M., 2017. Urban finescale forecasting reveals weather conditions with unprecedented detail. Bull. Am. Meteorol. Soc. 98, 2675–2688.

Sailor, D.J., Lu, L., 2004. A top–down methodology for developing diurnal and seasonal anthropogenic heating profiles for urban areas. Atmos. Environ. 38, 2737–2748.

Sailor, D.J., Vasireddy, C., 2006. Correcting aggregate energy consumption data to account for variability in local weather. Environ. Model Softw. 21, 733–738.

Sri Lanka Railways, 2019. Administration Report – 2019. URL: https://railway.gov.lk/web/images/pdf/admin_report_2019.pdf.

Sri Lanka Sustainable Energy Authority (SLSEA), 2017. Energy Balance – An Analysis of Energy Sector Performance. URL: http://www.energy.gov.lk/images/energy-balance/energy-balance-2017.pdf.

Sri Lanka Travel Guide, 2022. Banking Hours and Business Hours in Sri Lanka. URL. https://www.srilankatravel-guide.com/travel-information/formalities-regulations/business-hours/.

Stewart, I.D., Kennedy, C.A., 2017. Metabolic heat production by human and animal populations in cities. Int. J. Biometeorol. 61, 1159–1171.

Stewart, I.D., Oke, T.R., 2012. Local climate zones for urban temperature studies. Bull. Am. Meteorol. Soc. 93, 1879–1900.

Takane, Y., Ohashi, Y., Grimmond, C.S.B., Hara, M., Kikegawa, Y., 2020. Asian megacity heat stress under future climate scenarios: impact of air-conditioning feedback. Environ. Res. Lett. 2, 015004.

World Bank (WB), 2022. World Development Indicators. URL: https://datahelpdesk.worldbank.org/knowledgebase/articles/906519-world-bank-country-and-lending-groups.

United Nations (UN), 2019. World urbanization prospects: The 2018 Revision (ST/ESA/SER.A/420). URL: https://www.un.org/development/desa/pd/sites/www.un.org.development.desa.pd/files/files/documents/2020/Jan/un_2018_wup_report.pdf>.

United States Federal Highway Administration (FHWA), 2016. Highway Statistics. URL: https://www.fhwa.dot.gov/policyinformation/statistics/2016/pdf/vm1.pdf.

Urban Development Authority (UDA), 2018. (compiled edition). Re-amendment to the City of Colombo development plan (amendment) – 2008. Extraordinary Gazette no. 2054/45 dated 18/01/2018 and Rectification by Extraordinary Gazette no. 2058/29 dated 14.02.2018. URL: https://www.uda.gov.lk/attachments/act/q31LejWXNw.pdf>.

Varquez, A.C.G., Kiyomoto, S., Khanh, D.N., Kanda, M., 2021. Global 1-km present and future hourly anthropogenic heat flux. Sci. Data 8, 1–14.

Ward, H., Grimmond, C., 2017. Assessing the impact of changes in surface cover, human behaviour and climate on energy partitioning across Greater London. Landsc. Urban Plan. 165, 142–161.

Xie, M., Liao, J., Wang, T., Zhu, K., Zhuang, B., Han, Y., Li, M., Li, S., 2016. Modeling of the anthropogenic heat flux and its effect on regional meteorology and air quality over the Yangtze River Delta region, China. Atmos. Chem. Phys. 16, 6071–6089.

Xie, X., Blunn, L., Sun, T., Ratnayake, R., Emmanuel, R., Perera, N., Lu, S., Luo, Z., Grimmond, S., 2024a. Indoor overheating risks of residential buildings in different neighbourhoods in Colombo, Sri Lanka. In prep.

Xie, X., Blunn, L., Sun, T., Ratnayake, R., Emmanuel, R., Perera, N., Lu, S., Luo, Z., Grimmond, S., 2024b. The temporal and spatial population-based heat exposure during a heatwave in Colombo, Sri Lanka. In prep.

Xue, Y., Wang, Y., Peng, H., Wang, H., Shen, J., 2020. The impact of building configurations and anthropogenic heat on daily urban air temperature cycles. Build. Environ. 169, 106564.